IOSR Journal of Engineering (IOSRJEN) **www.iosrjen.org**
ISSN (e): 2250-3021, ISSN (p): 2278-8719
Vol. 05, Issue 03 (March. 2015), ||V2|| PP 43-58

Numerical and Experimental Investigation on Frost Formation on Cold Cylinders

Kamal A. R. Ismail[1], Fatima A. Morais Lino[1], Carlos T. Salinas[1], Luiz Vicente Scalon[2], Raquel da Cunha Ribeiro da Silva[1]

[1]*Department of Energy, Faculty of Mechanical Engineering, State University of Campinas, UNICAMP, CEP 13083-860, Campinas (SP), Brazil. Phone: +55 19 35213376; Fax: +55 19 32893722.*
[2]*Depto de Engenharia Mecânica-FEB, Av. Luiz E. Carrijo Coube nº.14-01, Vargem Limpa ,17.033-360 - Bauru/ SP.*

Abstract:*This paper presents the results of a study to develop a fast calculation routine which enables the prediction of the frost layer growth and the deposition velocity in terms of the surface temperature of the cold body, the rate of flow of the humid air and the rate of flow heat transfer and mass transfer equation for the flow of wet air around a circular cylinder are formulated and solved and the results are presented in function of the surface temperature, mass flow rate of the humid air and the mass flow rate of the working fluid. In order to validate the model and the numerical predictions, an experimental rig is constructed and adequately instrumented. Experiments were realized and the results were composed with the numerical predictions to confirm the validity of the model.*

Keywords- *Frost; Frost predictions, Frost thickness; modeling of frost; measurements of frost*

I. INTRODUCTION AND BIBLIOGRAPHIC REVIEW

When humid air passes over cold surfaces the liquid particles are deposited over the surface in the form of crystals by complicated mechanisms of heat and mass transfer forming a porous layer. If the process of frost deposition continues for long periods this may lead to the formation of thick glacial layer of frost which impairs the performance of the equipment and increases the pressure losses. In these cases the formed frost may be removed by a variety of methods causing additional heat gains and the usual undesirable interruption of the cooling process. For these and other reasons it is necessary to study deeply the process of frost formation to be able to operate the equipments efficiently and for long periods.

One of the first experimental studies on frost formation was realized by [1] in which the effects on the heat transfer and pressure drop were evaluated [2] estimated the effects of the frost growth on the energy losses in air conditioning and refrigeration systems and found that about 20% of the total energy is spent in the defrost process. Other important experimental contributions are due to [3],[4],[5],[6], [7] and [8].

Mau et al. [9] reported data and empirical correlations of the frost growth and its properties in terms of the temperature of the flat plate, air temperature, humidity, and velocity.

Lee and Ro [10] studied the frost formation on the surface of a horizontal cylinder in a wet air stream and obtained results of the heat transfer flow rate around the cylinder, the effective thermal conductivity of the frost and the temperature distribution around the cylinder. Yang and Lee [11] proposed correlations for the frost deposition on the surface of the cylinder of the frost thickness, density, temperature of the surface of the frost layer.

The literature survey shows that during the last fifty years many models were proposed to describe the phenomenon of frost formation as the model due to [3] which is strongly based upon experimental data and empirical equations. Parish and Sepsy [12] proposed a model to formulate the frost formation around a cylinder which by the use of global balances in the equations of momentum, energy and concentration try to quantify and evaluate the process of frost formation. The model proposed by Jones and Parker [13] uses global balances and considers the variation of the internal properties of the frost layer which makes the balances more representative.

Hayashi et al.[14] elaborated a model which divides the process of frost formation into three successive periods, where the first is the one dimensional growth of the crystals, the second period is for three dimensional growth and the last period is the period of total development or nearly static growth.

Tokura et al. [7] elaborated a set of parameters which enables the determination of the effective thermal conductivity. Aoki et al. [15] studied the third period of Hayashi et al. model in great details.

Sami and Duong [16] proposed modifications in Jones and Parker model by using local frost properties to obtain better predictions. Padki et al. [17] proposed an approximate model for frost formation by the use of empirical correlations to estimate the heat and mass film coefficients. Sherif [18] presented a transient semi-empirical model for frost formation over a flat plate. The model estimates the surface temperature and the frost layer

growth using existent correlations for the heat transfer coefficient and Lewis' analogy to calculate the mass transfer coefficient.

Tao et al. [19] proposed a frost formation model on a flat plate. The model is based upon the basic equations of heat and mass transfer and empirical correlations. The model solves the problem of frost formation in two stages, the first stage of short duration one dimensional crystal formation followed by the second stage which uses the data from the first stage as entry values.

Scalon [20] solved the problem of frost formation over a vertical cylinder in a wet air stream. He used the equations developed by [19], but differently from Tao et al., he solved the flow field equations to determine the convection and diffusion coefficients between the flow and the surface of the frost layer.

Salinas [21] and Ismail and Salinas [22] studied the case of frost formation over a flat plate placed parallel to the direction of wet air flow by using a formulation based upon the average volume local technique and were able to calculate the local density, frost layer thickness, mass deposition rate and phases mass fraction. They compared their results with available experimental and numerical data. Later Ismail and Salinas [22] extended their work to treat the case of flow of humid air and frost deposition between two parallel plates.

Some recent experimental work was realized by [23] on the formation of frost on vertical cold cylinders of different arrangements including the case of two cylinders in series and three cylinders in a triangular geometrical arrangement.

This paper presents the results of an investigation to develop a calculation routine which enables the prediction of the frost layer growth rate and the thickness of the frost layer under different operational conditions of mass flow rate of the working fluid, the surface temperature of the cold surface and the mass flow rate of the humid air. Experiments were realized on an experimental rig designed and instrumented to enable the variation of the air flow rate, the secondary working fluid flow rate and its temperature. The frost interface position was determined by a digital camera. The photographs were discretized to determine the real frost interface position. The experimental frost thickness and the frost deposition velocity were used to validate the numerical model and the numerical predictions.

II. FORMULATION OF THE PROBLEM

The mathematical model developed by [20] based upon [19] with some adaptation, was used in the present work to describe the process of frost formation around a vertical cold cylinder placed in a wet air stream. Accepting the model due to [19] ,at the moment is the most accepted model even it is not exact one, that the process of frost formation can be divided into two stages, where the first stage is one dimensional crystal growth followed by the second stage of interaction between neighboring crystals forming a porous matrix. Both Tao et al. and [20] used an empirical parameter called the transition time taken as 2/3 of the transition time given by [14]. The transition time is a parameter which indicates the transition predominance from one phase to the other, given in Fig. 1.

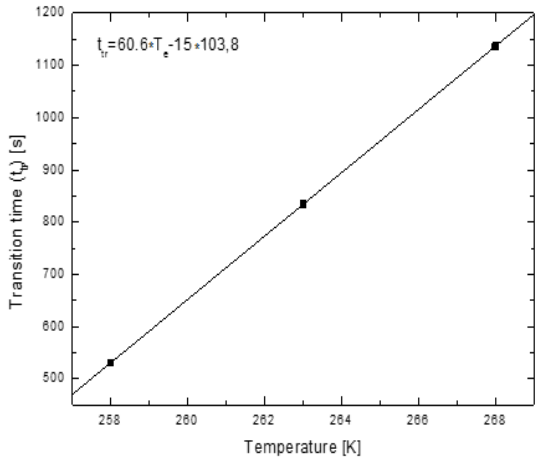

Fig.1 Values of transition times in the range of -20°C the 0°C.

1.1 ONE DIMENSIONAL CRYSTAL GROWTH

In this stage ice nucleus are formed on the cold surface and grow in the vertical direction as a consequence of the heat and mass transfer.

Following the model proposed by [19], the crystal growth is normal to the surface as shows in Fig. 2. Applying the energy equation on the element shown in Fig. 2.

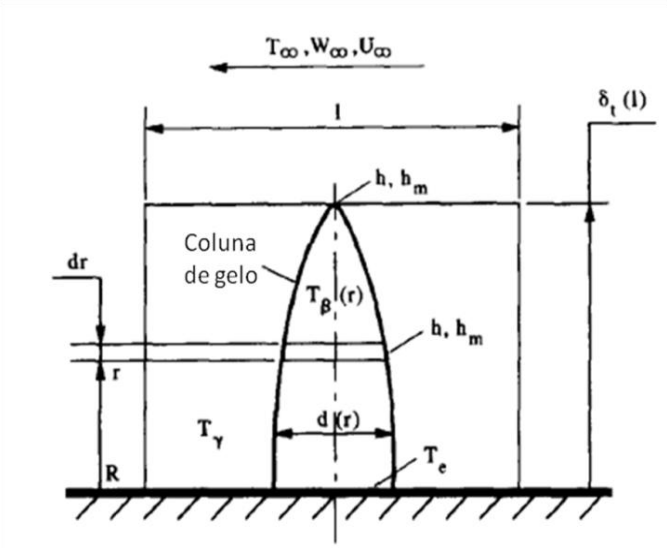

Fig. 2 Physical model for the growth of the ice crystals, [19]

$$\rho_g c_{p,g} \frac{\partial T}{\partial t} \frac{\pi}{4} d^2 dr - \rho_g \lambda \frac{\pi}{4dt} \left[\left(d + \frac{\partial d}{\partial t} dt \right)^2 - d^2 \right] dr = q_r + q_{conv} - q_{r+dr} \tag{1}$$

$$\rho_g c_{p,g} \frac{\partial T}{\partial t} \frac{\pi}{4} d^2 \, dr - \rho_g \, \lambda \frac{\pi}{4} \, 2d \, \frac{\partial d}{\partial t} \, dr =$$
$$-k_\beta \left(\frac{\pi}{4} d^2 \right) \frac{\partial T}{\partial r} + h(\pi \, d \, dr)(T_\gamma - T_\beta) - \left\{ k_g \left(\frac{\pi}{4} d^2 \right) \frac{\partial T}{\partial r} + \frac{\partial}{\partial r} \left[k_g \left(\frac{\pi}{4} d^2 \right) \frac{\partial T}{\partial r} dr \right] \right\} \tag{2}$$

$$\rho c_{p,g} d \frac{\partial T}{\partial t} = 4h(T_\gamma - T_\beta) + \frac{1}{d} \frac{\partial}{\partial r} \left(k_g d^2 \frac{\partial T}{\partial r} \right) + 2\rho_g \lambda \frac{\partial d}{\partial t}$$
$$\rho c_{p,g} d \frac{\partial T}{\partial t} = 4h(T_\gamma - T_\beta) + 2k_g \frac{\partial d}{\partial r} \frac{\partial T}{\partial r} + k_g d \frac{\partial^2 T}{\partial r^2} + 2\rho_g \lambda \frac{\partial d}{\partial t} \tag{3}$$

Applying the mass diffusion equation one can obtain

$$\left[\rho_g \frac{\pi}{4dt} \left(d + \frac{\partial d}{\partial t} dt \right)^2 - d^2 \right] dr = h_m (\pi d dr)(W_\gamma - W_\beta) \tag{4}$$
$$\rho_g \frac{\pi}{4} 2d \frac{\partial d}{\partial t} dr = h_m (\pi d dr)(W_\gamma - W_\beta) \tag{5}$$

Where W_β indicates the concentration evaluated at the temperature T_β of the solid phase and the result is:

$$\rho_g \frac{\partial d}{\partial t} = 2 \, h_m (W_\gamma - W_\beta) \tag{6}$$

These two equations represent the model for the first stage. The initial and boundary conditions necessary to solve this model are

When r = δ

$$d = d_0 \tag{7}$$

$$-\rho \lambda d_0 \frac{\partial \delta}{\partial t} = k_g d_0 \frac{\partial T}{\partial r}\Big|_\delta + h d_0 (T_\infty - T_s) \frac{\partial T}{\partial r}\Big|_\delta = \frac{h}{k_s} (T_\infty - T_s) + \frac{\rho_g \lambda}{k_g} \frac{\partial \delta}{\partial t} \tag{8}$$
$$\rho_g d_0 \frac{\partial \delta}{\partial t} = h_m (W_\infty - W_\delta)$$

$$\frac{\partial \delta}{\partial t} = \frac{h_m}{\rho_g} (W_\infty - W_\delta) \tag{9}$$

When r = 0

$$T_s = T_e \tag{10}$$

$$\frac{\partial d}{\partial t} = 0 \tag{11}$$

When t = 0

$$d = d_0 \tag{12}$$

$$\delta = \delta_0 \tag{13}$$

$$T_\delta = T_e \tag{14}$$

It is worth mentioning here that the gas phase temperature T_γ is function of the ambient temperature T_∞ and the cylinder surface temperature T_β, and the factor α whose value, according to [19], varies between zero for small values of Reynolds number and 1 for large values of Reynolds number.
Thus

$$T_\gamma = \alpha T_\infty + (1 - \alpha) \tag{15}$$

Since the nucleation phenomenon is not well understood, we adopted here that each control volume contains only one nucleus and hence we can write

$$d_0 = K_{frac}$$

where K_{frac} is the size of the control volume along the direction parallel to the surface and has the values as shown in Table 1 where ΔC is given in kg/m^3. It is important to mention that δ_0 cannot be zero because of numerical reasons, and in the present study a small value given by $\delta_0 = \frac{d_0}{30}$ is adopted.

Table 1 Adopted values of K_{frac}.

$\Delta C < 0.008$	$0.008 < \Delta C < 0.01$	$0.01 < \Delta C < 0.013$	$\Delta C > 0.013$
0.5	0.65	0.7	0.75

The frost formation model divided the process artificially into two stages, but the real formation process is a continuous one and the ice column are transformed into porous mesh of different structures. Hence a set of coupling equations are necessary to adequate the results of the first stage of column structure as entries to the second stage of frost formation.

These coupling equations are:

The volumetric fraction $\varepsilon_{\beta,i}$ is given by

$$\varepsilon_{\beta,i} = \frac{\pi d_i^2}{4l^2} \tag{16}$$

The temperature T_i can be evaluated by

$$T_i = \varepsilon_{\beta,i} T_\beta + (1 - \varepsilon_{\beta,i}) T_\gamma \tag{17}$$

The density $\rho_{f,i}$ and the specific heat $c_{p,i}$ are evaluated by

$$\rho_{f,i} = \varepsilon_{\beta,i} \rho_\beta + (1 - \varepsilon_{\beta,i}) \rho_\gamma \tag{18}$$

$$c_{p,i} = \varepsilon_{\beta,i} c_{p,\beta,i} + (1 - \varepsilon_{\beta,i}) c_{p,\gamma,i} \tag{19}$$

1.2 THE CRYSTALS SPREADING PHASE

As mentioned before, in this phase the crystals are spread over the cold surface forming a porous medium. This model is subject to some restrictions such as heat and mass transfer are one dimensional;

- constant internal pressure in the porous medium;
- thermal equilibrium among the phases;
- dominant thermal diffusion in relation to convection; and,
- Saturated air in the porous medium.

Considering a control volume in the porous medium, as shown in Fig.3 one can write the energy balance in the form

$$\rho_f c_{p,f} \frac{\partial T}{\partial t} + \dot{m}\lambda = \frac{\partial}{\partial r}\left(k_{ef} \frac{\partial T}{\partial r}\right) \tag{20}$$

The mass balance for a control volume

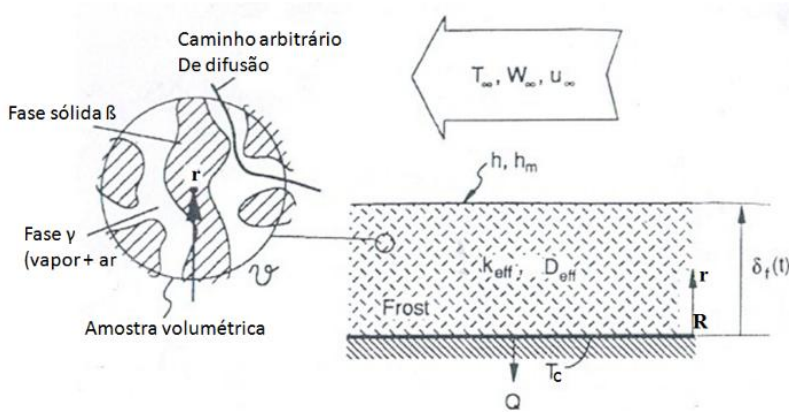

Fig. 3 Control volume representation in the porous medium after [19].

Phase γ

$$\frac{\partial \varepsilon_\gamma W}{\partial t} = \frac{\partial}{\partial r}\left(D_{ef} \frac{\partial W}{\partial r}\right) \tag{21}$$

Phase β

$$\frac{\partial \varepsilon_\beta}{\partial t} = \dot{m} = W - W_{sat} \tag{22}$$

Equations (20) to (22) represent the second stage model. By using adequate initial and boundary conditions these equations can be solved.

It is important to mention that for the solution the equations (20) to (22) the coupling equations (16) to (19) are used to adapt the results of the first stage to be used as entry values for the second stage.

The boundary conditions are:

On the surface of the cylinder r = 0,

$$T_s = T_e$$

$$\frac{\partial \varepsilon_d}{\partial r} = 0$$

The conditions at the moving frost interface at

$$r = \delta$$

$$h_m(W_\infty - W_\delta) = D_{ef,s} \frac{\partial W}{\partial r} + \rho_{f,s} \frac{\partial \delta}{\partial t} \tag{23}$$

$$h(T_\infty - T_s) = k_{ef} \frac{\partial T}{\partial r} - \rho_{f,s} \lambda \frac{\partial \delta}{\partial t} \tag{24}$$

$$\frac{\partial \varepsilon_\delta}{\partial r} = 0$$

The relevant thermal properties of the frost and air are obtained from the literature as below:

- The thermal conductivity k_g [24]

$k_g = \frac{630}{T}$[W/mK], where T in K. (25)

- The specific heat $c_{p,g}$ [24]

$c_{p,g} = 2116.56 + 7.284510^{-3}T$ [kJ/kgK], where T in K. (26)

- Specific volume v_g [25]
- $v_g = 1.0907x10^{-3} + 1.4635x10^{-3}T$[m³/kg], where T in K. (27)

- The density ρ_g [16]

$\frac{1}{\rho_g} = 0.0010907 + 1.4635x10^{-7}T$[kg/m³], where T in K. (28)

The properties of dry air are obtained from [25].

- The thermal conductivity k_{ar}

$k_{ar} = 0.001968 + 8.15x10^{-5}T$ [W/mK], where T in K. (29)

- The specific heat $c_{p,ar}$

$c_{p,ar} = 1.004$ [kJ/kgK], where T in K .(30)

- The density ρ_{ar}

$\rho_{ar} = \frac{344.9}{T}$ [kg/m³], where T in K. (31)

The effective diffusion coefficient is evaluated using [19]

$D_{ef} = \varepsilon_\gamma D(1 + F)[m^2/s]$ (32)

where D is the binary diffusion coefficient evaluated from

$D = 2.19\left(\frac{T}{T_0}\right)^{1.81} 10^{-5}$ [m²/s] (33)

- The effective diffusion coefficient on the surface is

$D_{eff} = \varepsilon_\gamma D(1 + F_s)$ [m²/s] (34)

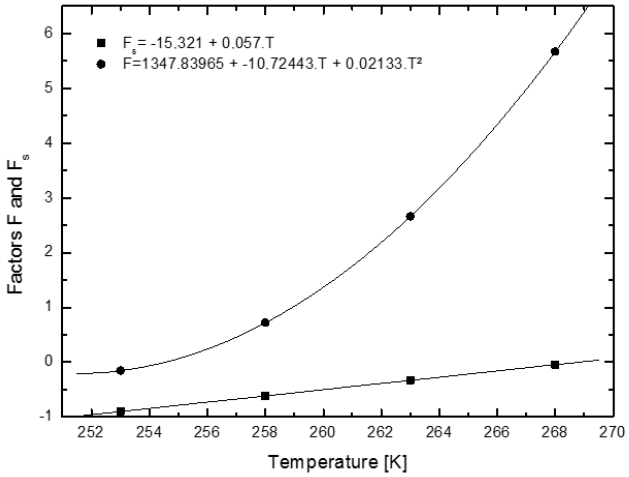

Fig. 4 Factors F and F_s as a function of temperature, [19].

where F and Fs are given by [19] and shown in Fig. 4.

- The saturation humidity of the air is

$W = 0.6218\frac{P_{vap,sat}}{P_{total} - P_{vap,sat}} =$ (35)

- The saturation pressure at any position in the frost layer is evaluated from [17],

$$\ln\left(P_{vap,sat}\right) = \frac{C_1}{T} + C_2 + C_3 + C_4T^2 + C_5T^3 + C_6T^4 + C_7\ln(T) \quad (36)$$

where

C1 = $-5.674\,535\,9\,10^3$
C2 = 6.392 524 7
C3 = $-9.677\,843\,0\,10^{-3}$
C4 = $6.221\,570\,1\,10^{-7}$
C5 = $2.074\,782\,5\,10^{-9}$
C6 = $-9.484\,024\,0\,10^{-13}$
C7 = 4.1635019

Equation (36) is valid for the interval -100°C<T<0°C where T is in K and $P_{vap,sat}$ is in Pa

- The total specific volume is,

$$v = 1.611168.\,10^{-2}\frac{T}{P}\left(1 + \frac{P_{vap}}{P}\right) \quad [m^3/kg] \quad (36a)$$

- The value of the sublimation latent heat, [12]

$$\lambda = h_{vap,T} - h_{ice,T} = -0.195386.T[k] + 2837.77 \quad [kJ/kg] \quad (37)$$

The effective thermal conductivity is evaluated by using the model due to [24], where the frost is treated as a porous medium of volumetric fraction ε given by

$$\varepsilon = \frac{\rho_g - \rho_f}{\rho_g - \rho_a} \quad (38)$$

The effective thermal conductivity is evaluated by

$$k_{ef} = \frac{1}{4}\left\{(3\varepsilon_c - 1)k_1 + (3x_c - 1)k_u + \sqrt{[(3\varepsilon_c - 1)k_1 + (3x_c - 1)k_u]^2 + 8\,k_l k_u}\right\} \quad (39)$$

Where

$k_u = (1-\varepsilon)k_b + \varepsilon k_c$ (Upper limit)
$k_1 = (1-\varepsilon)k_p + \varepsilon k_s$ (Lower limit)

Let us define

$$a = \frac{k_{e,ar}}{k_{ice}}$$

$$k_{e,ar} = k_{ar} + \frac{T_S k_v}{\varepsilon}$$

$$T_S = \frac{1}{(1+F_s)}$$

where

(a) Contribution due to air bubbles (k_b):

$$k_b = k_g\frac{1 - 2\varepsilon\left(\frac{1-a}{2+a}\right)}{1 + \varepsilon\left(\frac{1-a}{2+a}\right)}$$

(b) Contribution due to the frost cylinders(k_c):

$$k_c = (1-\varepsilon)k_g + \varepsilon k_{e,ar}$$

(c) Contribution due to the frost spheres(k_s):

$$k_s = k_g\frac{3 + \varepsilon(a-1)}{3 - \varepsilon\left(\frac{a-1}{a}\right)}$$

(d) Contribution due to the flat plate frost(k_p):

$$k_p = \frac{k_g k_{e,ar}}{(1-\varepsilon)k_{e,ar} + \varepsilon k_g}$$

The value of ε_c is given by the correlation obtained from experimental data:

$$\varepsilon_c = 13.6(\varepsilon_2 - \varepsilon_1)(\varepsilon - \varepsilon_1)^2 \left[1 - \frac{2}{3}\frac{\varepsilon-\varepsilon_1}{\varepsilon_3-\varepsilon_1} + \frac{\varepsilon-\varepsilon_1}{\varepsilon_2-\varepsilon_1} + \frac{(\varepsilon-\varepsilon_1)^2}{2(\varepsilon_3-\varepsilon_1)(\varepsilon_2-\varepsilon_1)}\right]$$

Where

$$\varepsilon_1 = 0.1726\left(\frac{T}{273.16}\right)$$

$$\varepsilon_2 = 0.751$$

$$\varepsilon_3 = 0.3sin\left\{\frac{\pi}{2}\left[\frac{1-\left(\frac{T}{273.16}\right)}{1-\left(\frac{T_e}{273.16}\right)}\right]\right\}$$

If $\varepsilon < \varepsilon_1$, then $\varepsilon_c = 0$. The value of x_c is defined as: $x_c = 1 - \varepsilon_c$.

The equations of the first stage, the coupling equations and the equations of the second stage together with the respective boundary and initial conditions were discretized by using the finite difference approximation. The numerical program was written in C++ and the numerical tests were realized to optimize the computational grid and make the results independent of the grid size. The value of dr was varied from 10^{-1} to 10^{-5} mm and dt from 10s to 10^{-4}s.

The predicted results were found to compare well with the experimental measurements for dr = 10^{-3} mm and dt = 10^{-2}s, and hence these values were used for all the present calculations.

III. EXPERIMENTAL MEASUREMENTS

In order to validate the model and the numerical predictions, an experimental rig was constructed and adequately instrumented, Fig.5. The experimental rig is composed of a wind tunnel with the test section made of acrylic sheet of 10mm thickness where the cold tube was fixed vertically and fed by the secondary fluid circuit. The air flow in the tunnel was controlled by varying the frequency of the driving motor, and the working section was calibrated such that both its mean velocity and the air flow rate are obtained in terms of the frequency of the driving motor. The humidity of the air was changed by using a commercial electric humidifier and the air was usually maintained as fully saturated. The circulating secondary fluid flow rate was measured by a calibrated orifice plate and its temperature at entry and exit of the cylinder were measured by calibrated thermocouples.

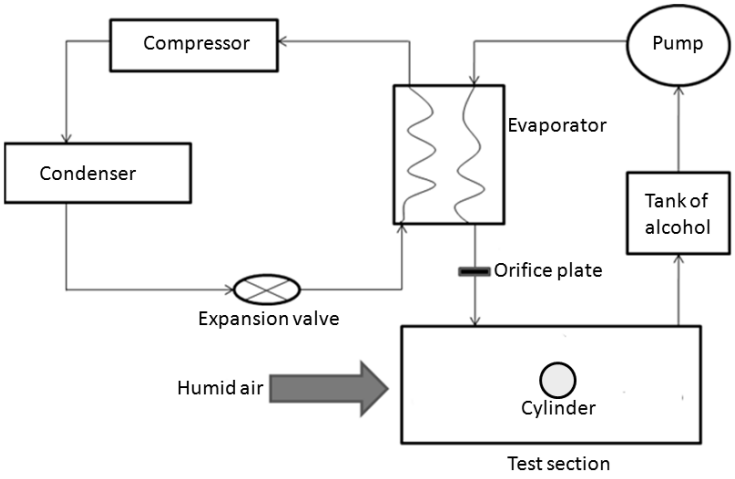

Fig. 5 Experimental rig.

The dry and wet bulb temperatures were measured before and after the test tube.

The deposition of frost on the surface of the cylinder was measured by photographing the cylinder by means of a high speed digital camera fixed normal to the cylinder axis. A precision measuring scale was fixed close to the cylinder and was always photographed together with the cylinder.

The uncertainty in the measurements and error propagation analysis were performed for all the experiments realized and the final values are listed in Table 2.

Table 2 Results of the uncertainty analysis

Quantity	Uncertainty
Time	$\delta_t = \pm 0.01s$
Frost thickness	e = $\pm 0.5mm$
Temperature	$\delta_T = \pm 0.5°C$
Humid air velocity	$\delta(v_{méd})i \pm \frac{0.01}{vméd}\, m/s$
Cylinder diameter	$\delta_{Dext} = \pm 0.0020mm$
	$\delta_{Dint} = \pm 0.0021mm$
Exit section of the wind tunnel	$\delta_A = \pm 0.91mm^2$
Air volume flow rate	$\delta_Q = \pm 0.00088m^3/s$
Air mass flow rate	$\delta_m = \pm 0.072163kg/s$
Secondary fluid	

At the beginning of the frost deposition process the temperature gradient between the surface of the cylinder and the air stream is big and consequently water droplets present in the wet air stream collide against the cold surface of the cylinder forming ice crystals. As the process continues more ice crystals are deposited over the cylinder surface forming a porous matrix. As the frost layer gets thicker it's the thermal resistance increases and the temperature difference decreases provoking the fusion of the solidified ice crystals and changing it to the liquid phase. When this occurs, the thermal resistance decreases and the liquid layer freezes and more ice particles are formed on the surface of the cylinder. This process is repeated many times and the final result is the formation of a layer of very dense frost or a layer of glacial ice. Figs.6 a,b show images of the frost porous layer and the frost glacial layer.

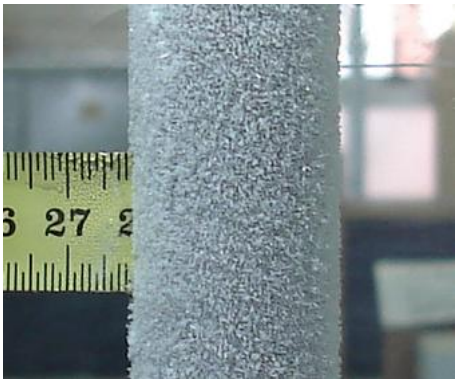

Fig. 6a Formation of the porous frost.

Fig. 6b Formation of the glacial frost.

IV. RESULTS AND DISCUSSION

As was mentioned before some numerical tests were realized to establish the optimum computational grids which make the numerical predictions independent of the grid size. The predicted test results were compared with the experimental measurements. It was found that $dr = 10^{-3} mm$ and $dt = 10^{-2} s$ gave good agreements with the experiments. Therefore these values were adopted for all the calculations.

Fig. 7 shows the variation of frost thickness with time and as function of the surface temperature of the cylinder. As can be seen the lower the surface temperature of the cylinder the thicker the frost layer for the same conditions and time.

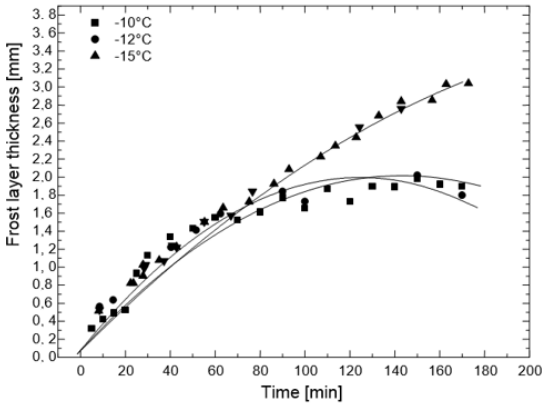

Fig.7 Variation of the frost layer thickness due to variation of the cylinder surface temperature for $\dot{V}_{ar} = 0.03\, m^3/s$ and $\dot{m}_{fsc} = 0.028 \frac{kg}{s}$.

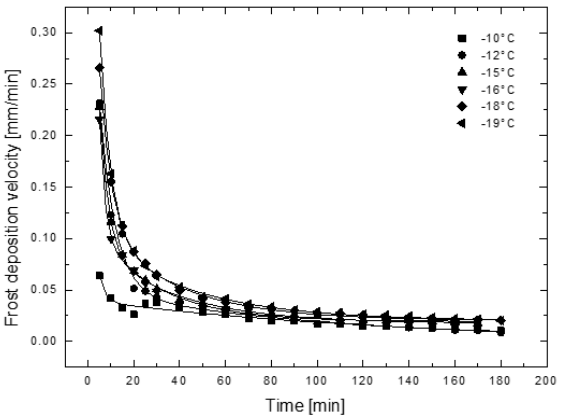

Fig.8 Variation of the frost deposition velocity due to variation of the cylinder surface temperature for $\dot{V}_{ar} = 0.03\, m^3/s$ and $\dot{m}_{fsc} = 0.028 \frac{kg}{s}$.

Fig.8. shows the variation of the frost deposition velocity with time and with the surface temperature of the cylinder. As can be seen, the lower the surface temperature of the cylinder the higher the frost deposition velocity. Also one can observe that the high initial frost deposition velocity due to the small initial thermal resistance. As the time goes on more frost is deposited the surface of the cylinder causing the increase of thermal resistance and consequently reducing of frost deposition velocity. The deposition of frost continues until towards the end of the process where the frost layer is so thick and the thermal resistance is too high so that the deposition velocity is very low and the frost deposition nearly stops.

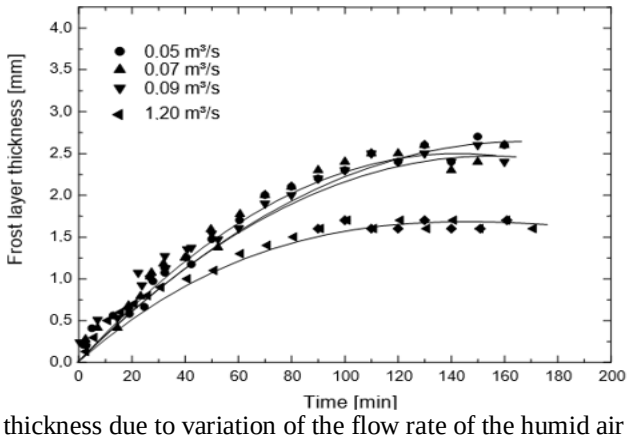

Fig.9 Variation of the frost thickness due to variation of the flow rate of the humid air for $T_{fsc} = -10\,^{o}C$ and $\dot{m}_{fsc} = 0.028\frac{kg}{s}$.

Fig. 9 shows the growth of the frost layer thickness with time for various wet air mass flow rates. As can be seen the increase of the wet air mass flow rate decreases of the frost layer thickness. This increase of the wet air mass flow rate increases the shear action on the layer, tearing off liquid particles and carrying it away with the air stream.

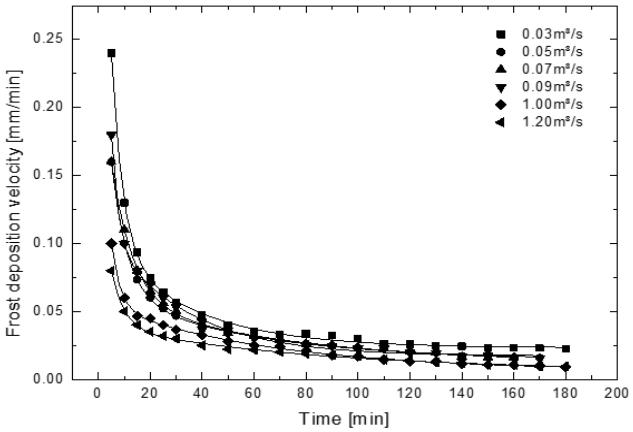

Fig.10 Variation of the frost deposition velocity due to variation of the flow rate of the humid air for $T_{fsc} = -10\,^{o}C$ and $\dot{m}_{fsc} = 0.028\frac{kg}{s}$.

The effect of the mass flow rate of humid air on the frost deposition velocity can be seen in Fig. 10. Where one can verify that high air flow rate reduces the deposition velocity. This effect can be explained by the shearing action of the high velocity, hence reducing the frost thickness and consequently the frost deposition velocity.

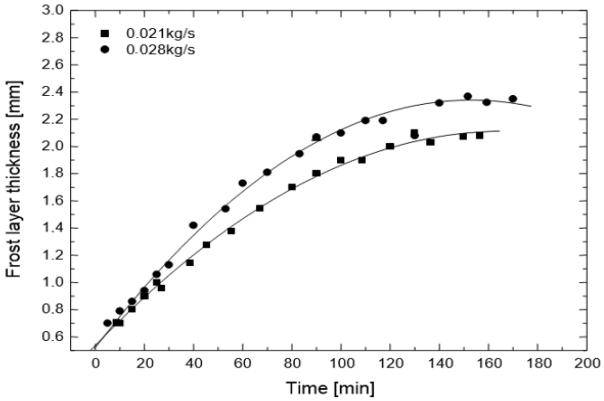

Fig.11 Variation of the frost thickness due to variation of the mass flow rate of the working fluid for $T_{fsc} = -10\,^{o}C$ and $\dot{m}_{fsc} = 0.028\frac{kg}{s}$.

Fig. 11 shows the effect of increasing the mass flow rate of the secondary fluid on the frost thickness. It is found that increasing the mass flow rate, leads to increase the internal heat transfer coefficient and hence reduces the thermal resistance, increases the temperature gradient and the deposition of frost.

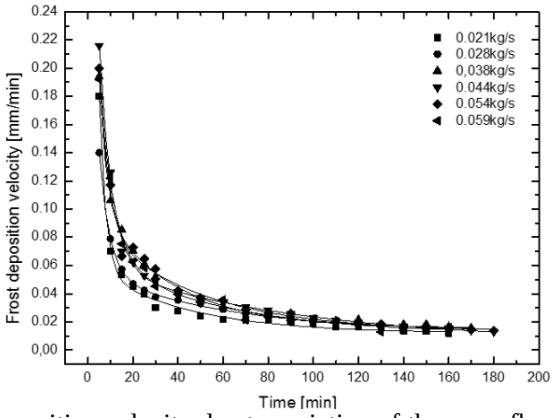

Fig. 12 Variation of the frost deposition velocity due to variation of the mass flow rate of the working fluid for $T_{fsc} = -13\,^{o}C$ and $\dot{V}_{ar} = 0.028\frac{kg}{s}$.

Fig. 12 shows that increasing the secondary mass flow rate, increases the internal heat transfer coefficient, increases the heat removal rate and hence increases the deposition velocity.

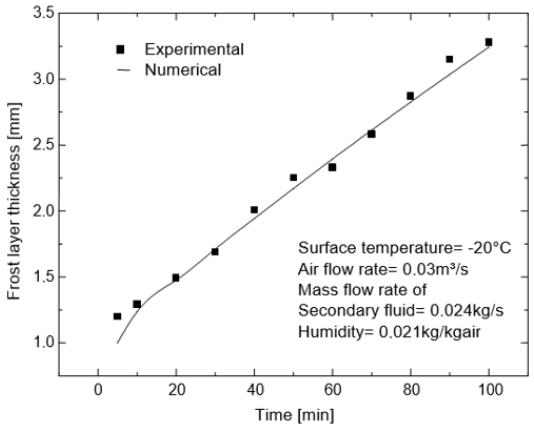

Fig.13 Comparison between the predicted frost thickness and the experimental measurements.

Fig.13. shows a comparison between predicted frost thickness and the experimental measurements. As can be seen the agreement is relatively good indicating that the model and the predicted results can be used for preliminary analysis of the frost deposition problem.
Fig.14 shows the variation of the frost deposition velocity with time both numerically and experimentally. As can be seen the agreement is good over the whole period.

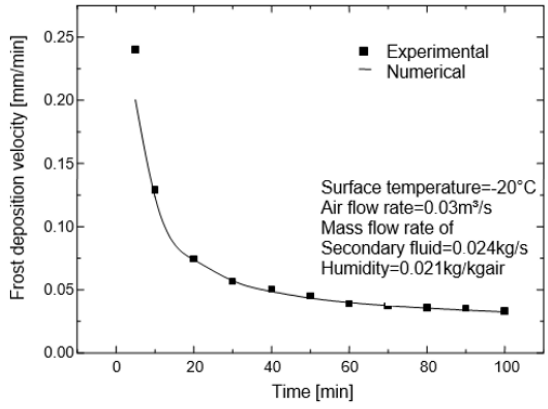

Fig.14 Comparison between the predicted frost deposition velocity and the experimental measurements.

Fig. 15 shows a comparison between the predicted frost thickness and frost deposition velocity and the experimental measurements. As can be seen the agreement is good. One can observe some abrupt change in the inclination of the numerically predicted thickness. This variation is only numerical due to the effect of the coupling model. The same can be said in relation to Fig. 16, which shows the predicted frost deposition velocity compared to the experimental measurements. One can observe the good agreement and the presence of the slight kink due to the coupling model.

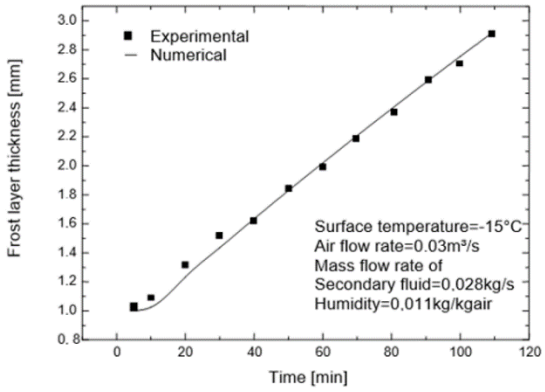

Fig.15 Comparison between numerical and experimental frost layer growth.

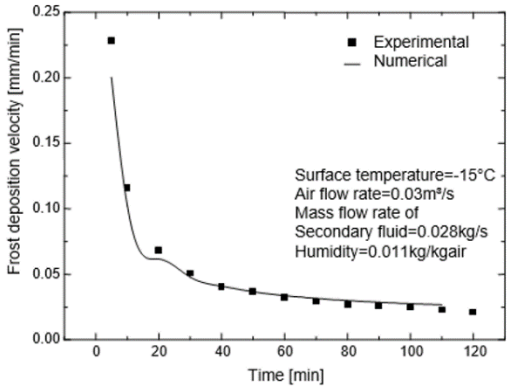

Fig.16 Comparison between numerical and experimental frost deposition velocity.

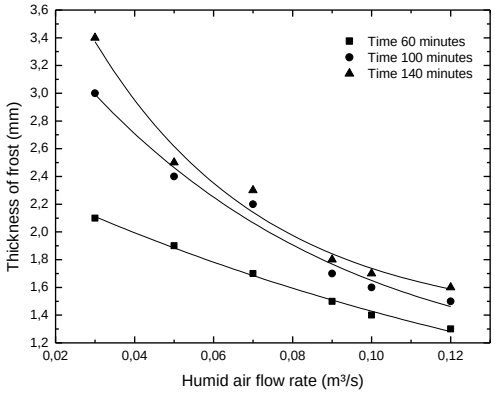

Fig.17 Effects of the humid air flow rate on the frost deposition rate for -10°C and 0.028kg/s.

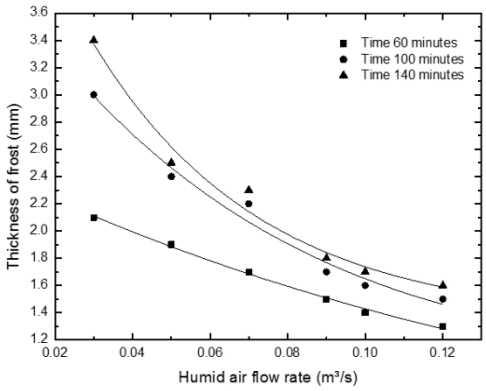

Fig.18 Effects of the humid air flow rate on the frost deposition rate for -10°C and 0.028kg/s.

Fig. 17 and 18 show the effect of the humid air mass flow rate on the frost thickness and deposition velocity. It is found that the increase of the wet air mass flow rate leads reducing the frost thickness and the deposition velocity because of the shearing action on the frost surface.

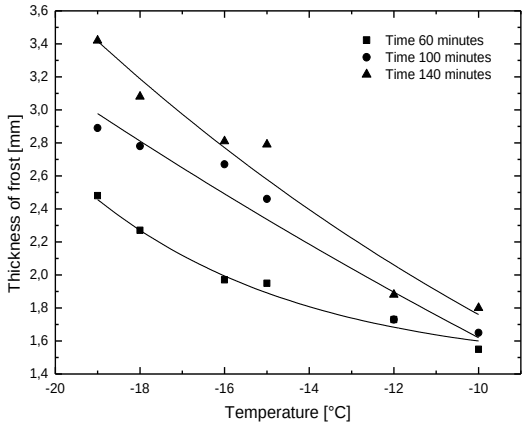

Fig. 19 Effects of temperature of the cold surface on the frost deposition rate for 0.03m³/s and 0.028kg/s.

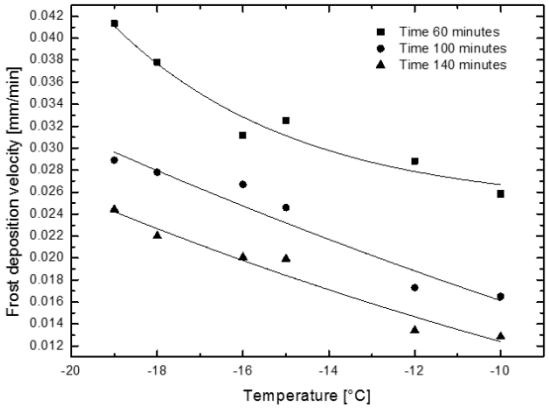

Fig. 20 Effects of temperature of the cold surface on the frost deposition rate for 0.03m³/s and 0.028kg/s.

Fig. 19 shows the effect of the surface temperature of the cylinder on the thickness of the frost layer. As can be seen lowering the surface temperature of the cylinder increases the temperature gradient and hence increases the deposition of frost on the surface of the cylinder. As the time goes on the rate of deposition is slowed down as can be seen from the decrease of the inclination of the deposition curve.

Fig. 20 shows the effect of the cylinder surface temperature on the frost deposition velocity. As can be seen, lowering the surface temperature leads to increase the deposition velocity.

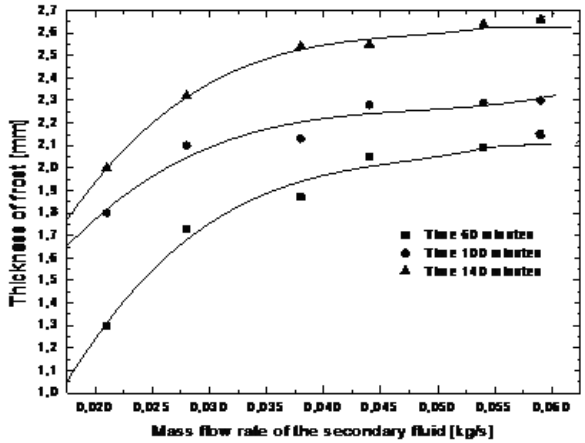

Fig.21 Effects of mass flow rate of the secondary fluid on the frost deposition rate for -13°C and 0.03m³/s.

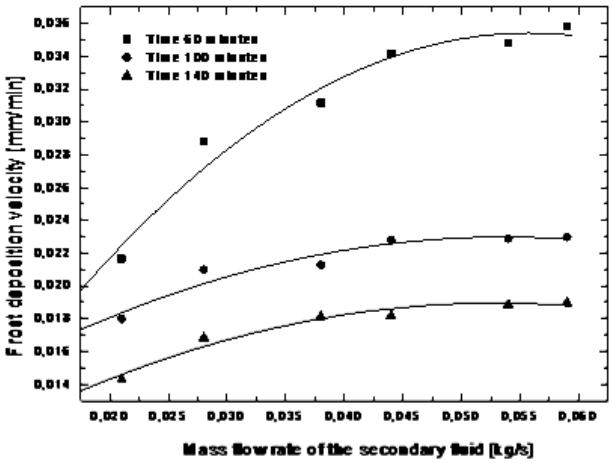

Fig.22 Effects of mass flow rate of the secondary fluid on the frost deposition rate for -13°C and 0.03m³/s.

Figs. 21 and 22 show the effect of increasing the secondary fluid mass flow rate. A can be seen increase the secondary fluid mass flow rate increases the internal Reynolds number and hence the internal coefficient of heat transfer. This leads to increasing the frost thickness and the frost deposition velocity.

V. CONCLUSIONS

Based upon the results and discussion, one can make the following conclusions.

1. The frost layer thickness and the frost deposition velocity decrease with the increase of the volumetric flow rate of the wet air.
2. The decrease of the cylinder wall temperature increases the frost layer thickness and increases the frost deposition velocity.
3. The increase of the mass flow rate of the secondary fluid circulating into the cold cylinder increases the frost deposited thickness and the frost deposition velocity.
4. The comparisons between the numerical predictions and the experimental results show relatively good agreement and thus validating the model and numerical predictions. This allows using the model for preliminary evaluation of frost formation.

VI. ACKNOWLEDGEMENTS

The authors wish to thank the CNPQ for the PQ research grant and the doctorate degree scholarship for the second author.

REFERENCES

[1] Stoecker WF. How the formation on coils affects refrigeration systems. Refrigerating Engineering 1957; 65 (2):42-46.
[2] Niederer DH. Defrosting of air units in central systems. ASHRAE Transactions. (1976)
[3] Chung PM, Algren AB. Frost formation and heat transfer on a cylinder surface in humid air cross flow. Heating piping and air conditioning 1958: (1) 171-178.
[4] Yonko JD, Sepsy CF. An investigation of the thermal conductivity of frost while forming on a fiat horizontal plate. ASHRAE Transaction 1967; 73: 1-10.
[5] Shah YT. Theory of frost formation. Ph.D. thesis, MIT 1969.
[6] Shneider HW. Equations of the growth rate frost forming in cooled surfaces. International Journal Heat Mass Transfer 1978; 21: 1019-1024.
[7] Tokura L, Saito H, Kishiuami K. Study on properties and growth rate of a frost layer on cold surfaces. International Journal Heat Mass Transfer 1983: 105: 895-901.
[8] Abdel-Whahed RM, Hifni MA, Sherif AS. Heat and Mass Transfer from a laminar humid air stream to a plate at subfreezing temperature. International Journal of Refrigeration 1984;7 (1).
[9] Mao Y, Besant RW, Falk J. Measurements and correlations of frost properties with laminar air flow at room temperature over a flate plate. ASHRAE Transactions: Symposia 1993: 739-745.
[10] Lee, Y. B., & Ro, S. T. (2001). An experimental study of frost formation on a horizontal cylinder under cross Flow Â rimentale sur le formation de givre sur un cylindre Etude expe Âe horizontal dans des conditions de convection force, 24, 468–474
[11] Yang, D.-K., and Lee, K.-S. (2004), Dimensionless correlations of frost properties on a cold plate. International Journal of Refrigeration, 27(1), 89-96.
[12] Parish HC, Sepsy CF. A numerical analysis of the frost formation under forced convsction. ASHRAE Transactions 1972: 236-251.
[13] Jones BW, Parker JD. Frost formation with varying environmental parameters. Journal of Heat Transfer 1975; 97: 255-259.
[14] Hayashi Y, Aoki A, Adaehi A, Hori K. Study of frost properties correlating with frost formation types. Journal Heat Transfer. 1977; 99: 239-245.
[15] Aoki K, Katayama K, Hayashi Y. A study on frost formation (the process of frost formation involving the phenomena of water permeation and freezing. Bulletin of JSME 1983; 26: 87-93.
[16] Sami SM, Duong T. Mass and heat transfer during frost growth. ASHRAE Transactions 1989; 95 (1): 158-165.
[17] Padki MM, Sherif SA, Nelson RM. A simple method for modeling frost formation in differents geometries. ASHRAE Transactions 1989; 95 (2): 1127-1137.
[18] Sherif SA, Raju SP, Padki MM, Chan AB. A semi- empirical transient method for modelling frost formation on a flat plate. International Journal of Refrigeration 1993;16(5):321–9.
[19] Tao YX, Besant RW, Mao Y, Rezkallah KS. Mathematical model for predicting the densification of frost on a fiat plate. International Journal Heat Mass Transfer 1993; 2: 353-363.
[20] Scalon VL. Formação de gelo em torno de cilindros verticais, Master thesis, Universidade Estadual de Campinas, 1993.
[21] Salinas CT. Formação de gelo em placa plana, Master thesis, Universidade Estadual de Campinas, Unicamp 1996.
[22] Ismail KAR, and Salinas CTS. Modeling of frost formation over parallel cold plates. International Journal of Refrigeration 1997; 22: 425-441.
[23] Martins KRSB. Estudo de formação de frost sobre tubos de diferentes arranjos em escoamento de ar úmido. Master Thesis, Universidade Estadual de Campinas 2010.
[24] Dietenberg MA. Generalized correlation of the water frost thermal conductivity. International Journal Heat and Mass Transfer 1983; 26 (4) 607-619.
[25] ASHRAE Handbook. Fundamentals the american society of heating refrigerating and air-conditioning engineers 1989. Atlanta, GA.